IMAGING RADAR POLARIMETRY FROM WAVE SYNTHESIS

Howard A. Zebker, Jacob J. Van Zyl, and Daniel N. Held
Jet Propulsion Laboratory, California Institute of Technology
Pasadena, California

I. INTRODUCTION

An imaging radar polarimeter measures the radar backscatter intensity and relative phase as a function of both the transmitted and received wave polarization states. We measure directly the amplitude and phase of all elements of the scattering matrix for each individual pixel in a radar image, and subsequent data processing combines these elements to synthesize any desired combination of transmit and receive antenna polarizations. Different scattering models predict different functional dependences of intensity on polarization--observation of this dependence for actual targets permits identification of the dominant scattering mechanisms contributing to the measured backscatter. For example, we find that Bragg scattering closely approximates the observed scattering from the ocean. Urban areas can be modeled as two-bounce dielectric corner reflectors.

Radar remote sensing provides information about the geometric and electric structure of an object. A conventional imaging radar measures a single value of reflectivity for many thousands of points in a scene for a single polarization, whereas observation with an imaging radar polarimeter can completely determine the dependence of reflectivity on polarization for each point in the scene. The radar polarization signature of an object permits stronger inferences of the physical scattering process than single-polarization measurements through identification and characterization of the dominant scattering mechanism, thus the solution for geometric shape and dielectric constant of an object is less ambiguous. The techniques required to generate arbitrary radar polarization through reconfiguration of system hardware have been known for some time, at least since Hagfors' (1967) lunar observations. This subject has recently been reviewed in some detail by Giuli (1986). A severe limitation of this approach is that the hardware must be modified for each observation, making it infeasible to measure the complete polarization signature of many points in a scene. Here we report a new approach to measurement of the complete polarization signature of an image implemented with an airborne synthetic aperture radar system: we utilize signals recorded on one data pass from orthogonal linearly-polarized antennas which we combine in the data processor to synthesize any desired combination of transmit and receive polarizations. This technique allows us to measure the complex, multichannel reflectivity of a scene on a single aircraft pass and later reprocess the data to provide multiple image maps, each representing the backscattered energy from the scene measured with a different combination of observational transmit and receive polarizations. The resulting polarization signature measurements indicate optimum polarizations for observations of certain classes of objects, and give insight into the identification of dominant scattering mechanisms for each kind of object. Knowledge of the scattering mechanism is helpful in providing an accurate description of the object of interest.

II. POLARIZATION OF THE TRANSMITTING AND RECEIVING ANTENNAS

We can denote the polarization state of the transmitting antenna by a complex 2-vector C_t such that

$$C_t = \begin{matrix} C_{t,x} \\ C_{t,y} \end{matrix} \tag{1}$$

Where $C_{t,x}$ is the phasor representation of the transmitted, complex (amplitude and phase) wave amplitude in the x direction, and $C_{t,y}$ represents the complex wave amplitude in the y direction when a unit voltage signal is applied to the antenna terminals. The wave amplitudes in equation (1) are related to the Stokes parameters s_i of the antenna by

$$\begin{aligned} s_0 &= |C_{t,x}|^2 + |C_{t,y}|^2 \\ s_1 &= |C_{t,x}|^2 - |C_{t,y}|^2 \\ s_2 &= |C_{t,x}|\ |C_{t,y}| \cos w \\ s_3 &= |C_{t,x}|\ |C_{t,y}| \sin w \end{aligned} \tag{2}$$

where w is the phase difference between $C_{t,x}$ and $C_{t,y}$. We list some of the more commonly used radar polarizations and their expression in terms of the above quantities in Table 1.

Simarily, we can describe the polarization of the receiving antenna by another 2-vector C_r, where $C_{r,x}$ represents the response of the antenna to a unit field aligned with the x direction and $C_{r,y}$ represents the response to a unit field aligned with y.

III. POLARIZATION CHARACTERISTICS OF THE SCATTERERS

We model the scattering behavior of an object as a two-by-two scattering matrix S with complex elements (see, for example, van de Hulst, 1980), that is, each element describes the relative magnitude and phase of the incident and scattered waves in the coordinate system described above, hence the matrix S includes the transformation from transmitted wave to received wave directions. In the most general case, element is a function of the angles of incidence and scattering, and the scattering matrix has the form

$$S = \begin{matrix} S_{xx}(r_i,d_i;r_s,d_s) & S_{xy}(r_i,d_i;r_s,d_s) \\ S_{yx}(r_i,d_i;r_s,d_s) & S_{yy}(r_i,d_i;r_s,d_s) \end{matrix} \tag{3}$$

with the elements of S defined as in the following example: The quantity $S_{xy}(r_i,d_i;r_s,d_s)$ represents the complex ratio

$$\frac{E_{s,x}(r_s,d_s)}{E_{i,y}(r_i,d_i)} \tag{4}$$

where $E_{i,y}$ is the y-component of the incident wave, for incidence direction $(r_i d_i)$, and $E_{s,x}$ is the x-component of scattered wave amplitude in the direction (r_s, d_s). The other elements of S are defined correspondingly, and several representative S-matrices for various scattering models are given in Table 2. Using the above definitions of C_t, C_r and S, we model the voltage V measured at the terminals of an antenna C_r in response to a wave initially generated by the antenna C_t, and subsequently scattered by an object characterized by S by

$$V = C_r^T \, S \, C_t \tag{5}$$

where the superscript T denotes the matrix transpose operation. Expanding the matrix multiplication (5), we have

$$V = C_{r,x} \, S_{xx} \, C_{t,x} + C_{r,x} \, S_{xy} \, C_{t,y} + C_{r,y} \, S_{yx} \, C_{t,x} + C_{r,y} \, S_{yy} \, C_{t,y} \tag{6}$$

The resulting received power P is then given by

$$P = V \, V^* \tag{7}$$

where the * denotes complex conjugation.

Note that using horizontally-polarized antennas (C_t = (1 0), C_r = (1 0)) for both transmit and receive functions permits inference of S_{xx} directly from our measurement V, as only the first term of (6) contributes. The remaining combinations of horizontal and vertical transmit and receive antennas yield each of the other elements S_{xy}, S_{yx}, and S_{yy}.

Knowledge of all elements of S then allows us to calculate the measured scattering behavior of an object in response to synthesized, arbitrary transmit and receive polarizations. For example, from the actual measured voltages S_{ij}, the polarization vectors of the desired antenna polarizations, and equation (10), we can express the voltage we would have measured with RCP ($C_t = (1/2^{1/2} \; (1 \quad i))$ transmit and LCP ($C_r = (1/2)^{1/2}(i \quad 1)$) receiving antennas as

$$\begin{aligned} V &= C_r^T(\text{LCP antenna}) \; S \; C_t \; (\text{RCP antenna}) \\ &= (1/2)^{1/2} \quad (i \quad 1) \begin{matrix} S_{xx} & S_{xy} \\ S_{yx} & S_{yy} \end{matrix} (1/2)^{1/2} \begin{matrix} 1 \\ i \end{matrix} \\ &= (1/2) \quad (i \quad 1) \begin{matrix} S_{xx} + iS_{xy} \\ S_{yx} + iS_{yy} \end{matrix} \\ &= (1/2) \quad (iS_{xx} - S_{xy} + S_{yx} + iS_{yy}) \end{aligned} \tag{8}$$

In this manner, we can determine the measured voltage, and hence the power corresponding to any arbitrary combination of transmit and receive polarizations utilizing only horizontally and vertically polarized antennas, if we employ equations of the form (6).

It is instructive at this point to consider a simple example of target backscatter behavior as a function of polarization in order to understand the basic operation of the polarimeter. The scattering matrix S that describes a unit-area isotropically scattering sphere is (van de Hulst, 1980)

$$S = \begin{matrix} 1 & 0 \\ 0 & 1 \end{matrix} \qquad (9)$$

The backscatter coefficient is unity for both of the diagonal elements of the scattering matrix, and zero for the off-diagonal elements. With this scattering matrix, equation (6) simplifies to

$$V = C_{r,x}\, C_{t,x} + C_{r,y}\, C_{t,y} \qquad (10)$$

We note that if the transmit polarization is horizontal (C_t = (1 0)) and the receive polarization is vertical (C_r = (0 1)), the response of the polarimeter will be zero. If RCP is chosen for transmit and LCP for receive ($C_t = (1/2)^{1/2}$ (1 i), $C_r = (1/2)^{1/2}$ (i 1)), however, the power received is maximized and equal to 1. Same-sense circular polarization for transmit and receive (RCP-RCP ro LCP-LCP) again yields zero power.

In summary, if our airborne hardware permits direct measurement of each element of S, through use of both horizontal and vertical antennas for transmit and receive, then these elements can be combined in the data processor to produce images representing any desired polarization state. Our imaging radar polarimeter thus consists of i) a conventional imaging radar with linear, orthogonally-polarized horizontal and vertical antennas, and ii) a data processor that can be used to synthesize the complete polarization signatures for each point in a scene.

IV. POLARIZATION SIGNATURES

Imaging radar polarimeter observation of an object with scattering matrix S yields a measured voltage V, and power P, as given by equations (6) and (7) above. Since this quantity depends on the polarization states C_t and C_r of the transmitting and receiving antennas, respectively, we can define the polarization signature of S as the variation of P as a function of the polarizations of the antennas. The most general representation allows arbitrary values for each of the transmitting and receiving polarizations.

We illustrate some typical polarization signatures by first calculating scattering matrices corresponding to several scattering models, and then displaying the signatures resulting from application of equations (6) and (7) to each model. The first is an isotropically-scattering sphere (see equation (9) above), the second is a Bragg model, and the third is a dihedral corner reflector made of a dielectric material that is applicable to modeling urban areas. We note that the Bragg model predicts higher reflectivity for vertically-polarized waves than for horizontally-polarized waves, while the dihedral model predicts the reverse.

Examination of the plots in Figure 1 corresponding to the isotropic sphere shows that for co-polarized imaging, linear polarization provides the greatest return, and that the signal strength is independent of linear polarization angle. This independence of linear polarization direction is a consequence of the lack of a preferred orientation for spheres. For the cross-polarization spectrum, signals are greatest for the circular polarizations and smallest for linear polarizations. The Bragg model is somewhat different in nature from the isotropic sphere models in that an enhancement for vertical polarization over horizontal polarization is evident in the co-polarized spectrum. Also, the co-polarized minimum occurs not at LCP and RCP but slightly towards linear polarization for each. This behavior is due to $|S_{yy}|$ exhibiting greater magnitude than $|S_{xx}|$. A dielectric dihedral corner reflector model exhibits a very different polarization signature from the previous two models. The co-polarized spectrum possesses two minima at linear polarizations offset by $\pm 45°$ from the x and y directions, and the cross-polarized spectrum possesses maxima at these locations.

We note that use of an imaging polarimeter to observe the full polarization signature of an object, coupled with interpretation in terms of simple scattering mechanisms such as those illustrated here, allows us to develop a scattering model that is consistent with the measured polarization properties of the object, even if we cannot exclude all other possible models. While we have clearly not considered all possible scattering models, it follows from the above that if the polarization signature of a real object could be unambiguously identified as resembling any one of the models depicted here, the dominant scattering mechanism may be described and analyzed with some confidence.

In Figure 2 we present polarimeter images in synthesized polarization combinations, and also present some complete polarization signatures of sub-areas of these images. The data shown here were processed by synthesizing a set of linear, co-polarized antennas and applying them to data collected over San Francisco, California. This figure consists of twenty images; the upper left image corresponds to horizontal transmit, horizontal receive polarization. Scanning from left to right and from top to bottom, the angle of the electric field vector is advanced 2.5° per image and the amplitude of the result is displayed. The lower right image thus corresponds to linear polarization oriented 47.5° from horizontal. We note that the urban area, for example, exhibits great variation in brightness as the polarization changes, while the Golden Gate Park area changes little. As we note in the discussion of the polarization signatures below, we can predict the variation of the urban area quite well using a two-bounce corner reflector model, while we interpret the relative constancy of the park as indicative of a higher degree of multiple scatter than is apparent elsewhere in the image.

Measurement of the brightness of any sub-area of an image as the polarization is varied yields the observed polarization signature of that region. The complete polarization signatures for each of three sub-areas are shown in Figure 3. The observed signature of the ocean closely resembles the Bragg signature of Figure 1b, thus it is likely that some Bragg-like mechanism is responsible for backscatter from the ocean. The urban polarization signature is similar in appearance to the dihedral model (Figure 1c), with the addition of a "pedestal" to the overall signature. The park signature

exhibits a still greater pedestal than does the urban signature. We ascribe this additive term to an unpolarized component in the observed backscatter, thus the signal from an urban area can be modeled as including a polarized, dihedral-type return plus an unpolarized component.

We have shown that it is possible to measure the complete scattering matrix of an object using data acquired on a single aircraft pass, and can combine the signals later in the data processor to generate radar images corresponding to any desired combination of transmit and receive polarization. Various scattering models predict different dependence on polarization state of received power from an object. Our imaging polarimeter permits determination of this dependence, which we call the polarization signature, of each point in a radar image. Comparison of the theoretical predictions and observational data yield identification of possible scattering mechanisms for each area of interest. We have found that backscatter from the ocean is highly polarized and well-modeled by Bragg scattering, while scattering from trees in a city park possesses a considerable unpolarized component. Urban regions exhibit the characteristics expected from dihedral corner reflectors and their polarization signatures are quite different from the one-bounce Bragg model.

REFERENCES

Giuli, D., Polarization Diversity in Radars, Proc. of the IEEE 74, 245-269, 1986.

Hagfors, T., A Study of the Depolarization of Lunar Radar Echoes, Radio Science 2,445-465, 1967.

Van de Hulst, H., Light Scattering by Small Particles, Dover Publications, New York, 1981.

Table 1. Some common radar polarizations

Polarization	Vector C	Complex polarization p	Stokes vector
Linear horizontal	(1 0)	0	(1,1,0,0)
Linear vertical	(0 1)	B	(1,-1,0,0)
Right-hand circular (RCP) $(1/2)^{1/2}$	(1 i)	i	(1,0,0,-1)
Left-hand circular (LCP) $(1/2)^{1/2}$	(i 1)	-i	(1,0,0,1)

Table 2. Representative S - matrices

Model	S-matrix	Notes
Isotropic sphere	$\begin{matrix} a & 0 \\ 0 & a \end{matrix}$	a real, a > 0
Bragg	$\begin{matrix} a & 0 \\ 0 & b \end{matrix}$	a,b real a >0, b >0 b > a
Real-dielectric dihedral corner reflector	$\begin{matrix} -a & 0 \\ 0 & b \end{matrix}$	a,b real a > 0, b >0

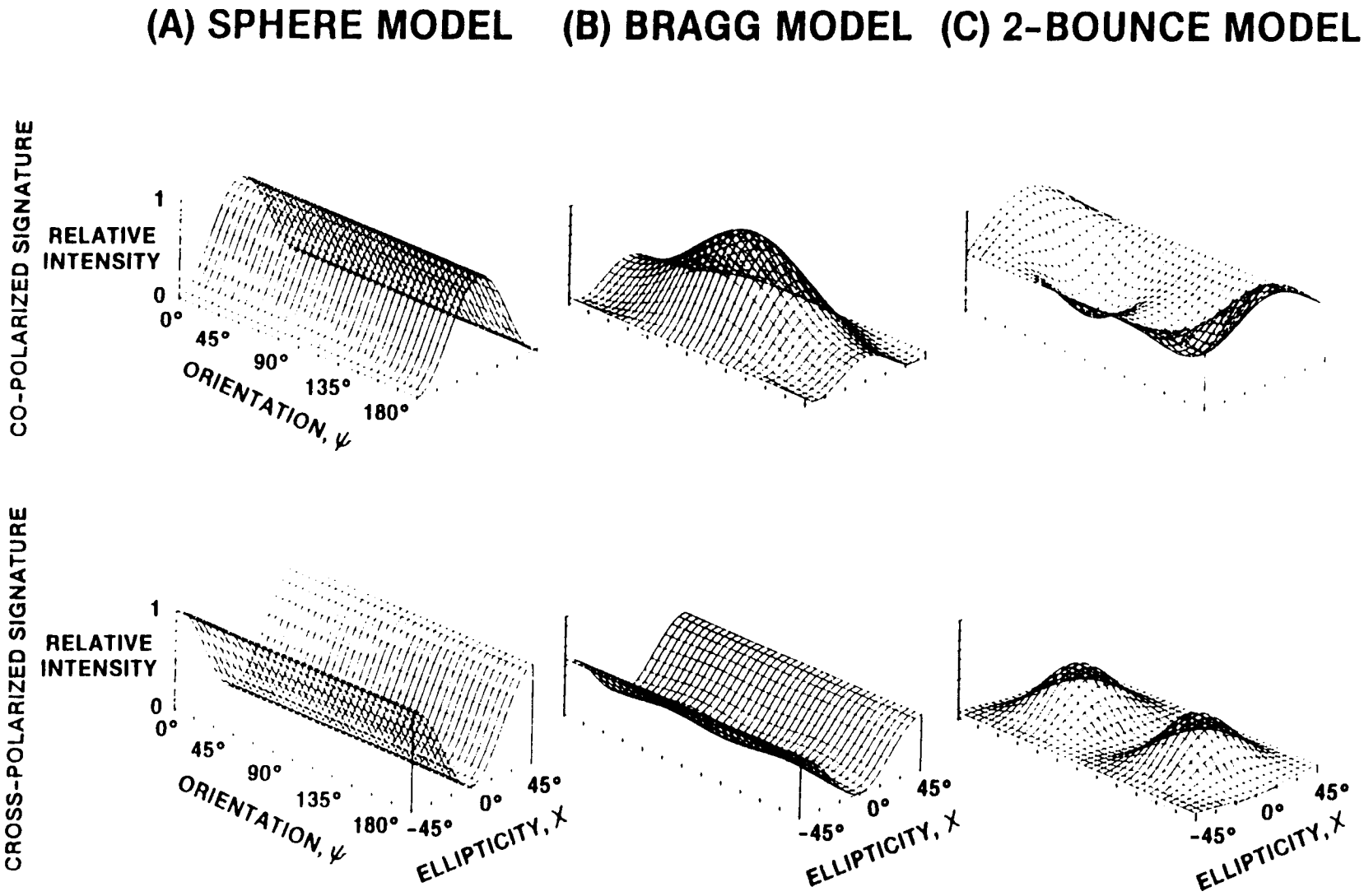

Figure 1. Plots corresponding to the isotropic sphere

Figure 2. Polarimeter images of San Francisco. The data shown were processed by synthesizing a set of linear, copolarized antennas and applying them to data collected over San Francisco, California

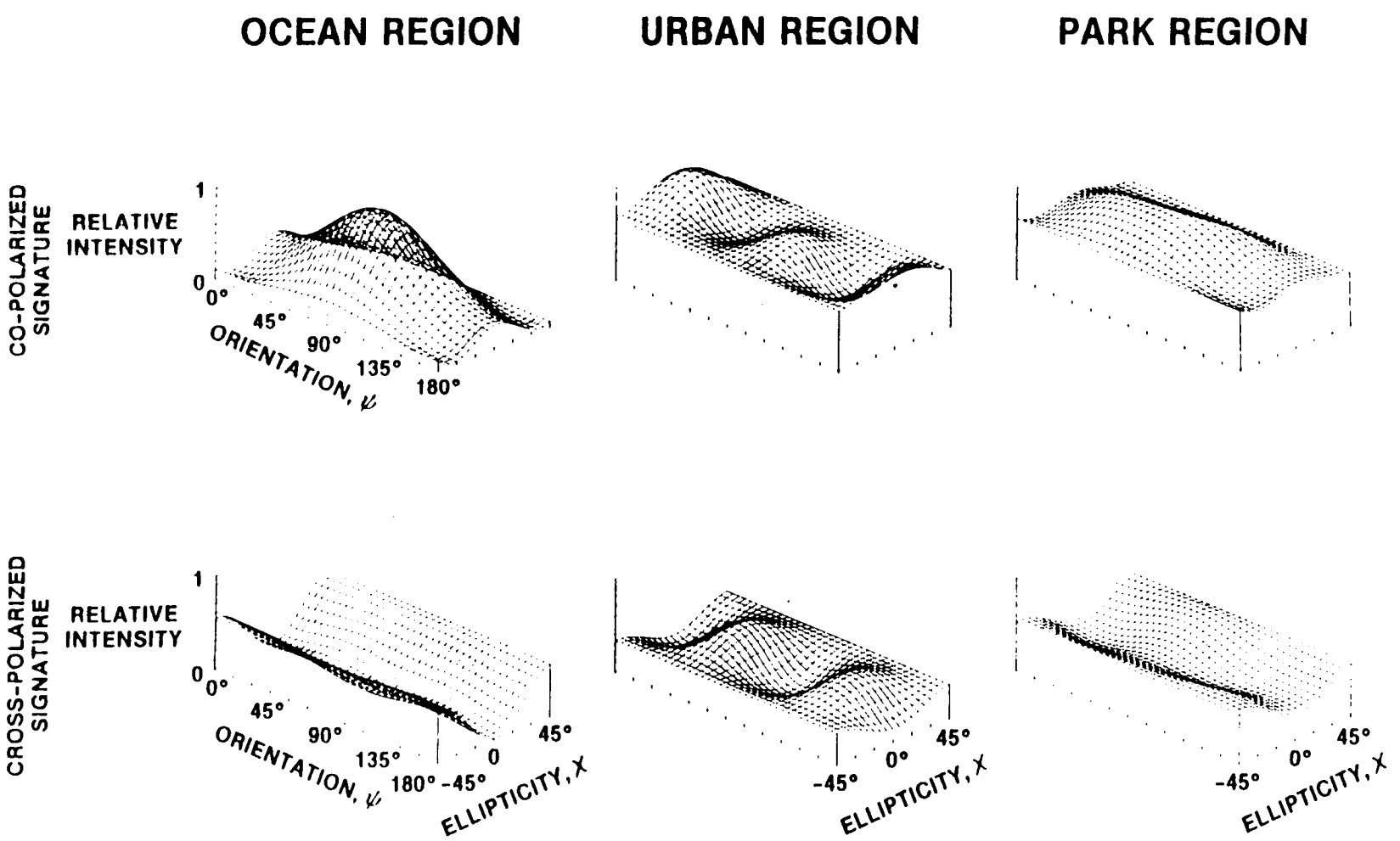

Figure 3. Complete polarization signatures